

# Benchmarking on improvement and site-adaptation techniques for modeled solar radiation datasets

Jesus Polo<sup>1</sup>, Carlos Fernández-Peruchena<sup>2</sup>, Vasileios Salamalakis<sup>3</sup>, Luis Mazorra-Aguilar<sup>4</sup>,  
Mathieu Turpin<sup>5</sup>, Luis Martín-Pomares<sup>6</sup>, Andreas Kazantzidis<sup>3</sup>, Philippe Blanc<sup>7</sup>, Jan Remund<sup>8</sup>

<sup>1</sup> Photovoltaic Solar Energy Unit (Energy Department e CIEMAT), Avda. Complutense 40, 28040 Madrid, Spain

<sup>2</sup> Spanish Center of Renewable Energies (CENER), Spain

<sup>3</sup> Laboratory of Atmospheric Physics, University of Patras, Greece

<sup>4</sup> SIANI, University of Las Palmas de Gran Canaria, Spain

<sup>5</sup> Reuniwatt SAS, 14 rue de la Guadeloupe, 97490 Sainte-Clotilde, France

<sup>6</sup> ISES member, PVPS-Task 16 participant

<sup>7</sup> Center O.I.E. Mines ParisTech Armines, France

<sup>8</sup> Meteotest, Fabrikstrasse 14, CH-3012 Bern, Switzerland

Corresponding Author:

Jesús Polo, email: [jesus.polo@ciemat.es](mailto:jesus.polo@ciemat.es), Phone: +34 914952513, Fax : +34 913466037

## Abstract

High-accuracy solar radiation data are needed in almost every solar energy project for bankability. Time series of solar irradiance components that spans decades can be supplied by satellite-derived irradiance or by reanalysis models, with very various types of uncertainty associated to the specific approaches taken and quality of boundary conditions information. In order to improve the reliability of these modeled datasets, comparison with ground measurements over a short period of time can be used for correcting some aspects, bias mainly, of the modeled data by using different methodologies; this procedure is known as site adaptation. Therefore, a benchmarking exercise that uses different site adaptation techniques was proposed within the Task 16 IEA-PVPS activities. In this work, over ten different site-adaptation techniques have been used for assessing the accuracy improvement, using ten different datasets covering both satellite-derived and reanalysis solar radiation data. The effectiveness of these methods is found not universal or spatially homogeneous, but in general, it can be stated that significant improvements can be achieved eventually in most sites and datasets.

34 Keywords: satellite-derived solar radiation, site adaptation, bankability of data for solar  
35 projects, modeled solar radiation data

## 36 **1. Introduction**

37 Solar power deployments, such as photovoltaics (PV) or concentrating solar power  
38 (CSP) plants, require high-quality decade-long time series of solar radiation data for  
39 both technical (planning dimensioning and designing stages) and financial aspects of  
40 the project. The long-term variability of solar resources plays a significant role in  
41 estimating the probability of exceedance of the future energy yields of a solar power  
42 plant, and it influences the financial conditions that the project is likely to receive  
43 (Fernández-Peruchena et al., 2018). Notwithstanding, due to the significant intra-day  
44 and inter-annual variability of solar irradiance, the solar resource assessment should  
45 consider time series, instead of only considering the climatological averages. Reliable  
46 and bankable solar radiation data should include at least time series of direct normal  
47 irradiance (DNI) for CSP projects, and global horizontal irradiance (GHI) or plane of  
48 array (POA) global irradiance for the PV ones (Sengupta et al., 2017). Additionally,  
49 high-quality diffuse horizontal irradiance (DHI) data are also desirable and might be  
50 required in specific solar projects and applications.

51  
52 Long-term time series of the solar radiation components at the Earth's surface can be  
53 modelled by many methodologies based on satellite imagery or numerical weather  
54 model reanalysis. The use of satellite-based models is currently most common in  
55 carrying out both solar resource mapping and site-specific solar irradiance data  
56 generation, since this approach has achieved a high degree of maturity and reliability.  
57 Solar engineers' extensive modeling experience in producing operational satellite-  
58 derived irradiance can be traced back to the late 1980s (Cano et al., 1986; Polo et al.,  
59 2008; Polo and Perez, 2019). The works that aim to validate, improve and apply these  
60 satellite-based methods are still on-going today and are being reported regularly in the  
61 relevant scientific and industry communities (Cros et al., 2019; Merrouni et al., 2017;  
62 Perez et al., 2017; Pfeifroth et al., 2017; Porfirio and Ceballos, 2017; Qu et al., 2017;  
63 Riihelä, 2018; Tang et al., 2016; Thomas et al., 2016; Urraca et al., 2017; Yang, 2019,  
64 2018; Yang and Boland, 2019; Yang and Perez, 2019). High-quality, satellite-derived  
65 irradiance datasets are made freely available by several providers, such as PVGIS  
66 (Amillo et al., 2014), CM-SAF (Kothe et al., 2019; Posselt et al., 2012), or NSRDB  
67 (Sengupta et al., 2018). In addition, the quality of the latest reanalysis data has  
68 improved significantly (Urraca et al., 2018), although the specific validation exercise  
69 was performed using daily data and the hourly results are still unclear. Nevertheless,  
70 large number of recent works highlights the interest on this topic (Feng and Wang,  
71 2019; Huld et al., 2018; Peng et al., 2019; Perdigoão et al., 2016; Ramirez Camargo and

72 Dorner, 2016; Salazar et al., 2020; Tahir et al., 2020; Trolliet et al., 2018; Zib et al.,  
73 2012).

74

75 That said, despite the improvements and quality gained in the recent years, various  
76 types of uncertainties are still embedded in modeled solar irradiance datasets,  
77 particularly owing to the uniformity of the data-generating process. Stated differently,  
78 when a model retrieves solar irradiance at a specific site some uncertainties are  
79 involved. Systematic errors in the models, limitations in the spatial and temporal  
80 resolutions, uncertainty in the atmospheric data that affects the radiative transfer  
81 process are, among others, some of the major sources of uncertainty that can result in  
82 biases or deviations in the modeled data.

83

84 Validation results in the literature for GHI and DNI, either satellite-derived or  
85 reanalysis-based, are very difficult to summarize. A huge amount of studies can be  
86 found elsewhere. Many providers and models report uncertainties that can vary a lot  
87 depending on the geographic area, the intrinsic characteristics of the model and on the  
88 quality of ground data used for validation. In order to illustrate this variability, just a  
89 few recent validation results are given next. Uncertainties in the range of -4 to 9%  
90 MBD (Mean Bias deviation) and 17-50% RMSD (Root Mean Square Deviation) for  
91 hourly GHI were reported with the eastern Meteosat satellite (Amillo et al., 2014). In  
92 India, SARA-E satellite-based estimations resulted in 10-20% overestimation of the  
93 surface incoming solar radiation (Riihelä, 2018). In Chile, nearly unbiased hourly GHI  
94 with 20% RMSD was recently estimated using GOES satellite imagery (Molina et al.,  
95 2017). Recent validation of the National Solar Radiation database (NSRBD) reported  
96 RMSD ranges of 9-18% and 15-30% for hourly GHI and DNI, respectively (Yang, 2018).  
97 The HelioClim-3 database reported 8% MBD and 20% RMSD for DNI estimations in  
98 Morocco (Merrouni et al., 2017). Version 4 of the SUNY model has improved notably  
99 its performance in both GHI and DNI (Perez et al., 2015). Therefore, quality, availability  
100 and completeness of the ground data, topography and climatology of the site,  
101 accuracy of the boundary conditions and input parameters (atmospheric composition,  
102 cloud properties, etc.) play an important role in the uncertainty characterization of the  
103 models for estimating solar radiation components.

104

105 In virtually every solar power project, and in many other applications, the preliminary  
106 characterization of long-term solar resources is done by evaluating the modeled time  
107 series of solar irradiance against short-term local ground measurements. Setting up a  
108 high-quality, ground-based monitoring station at the project site is always  
109 recommended for projects with significant financial investment. It is also highly  
110 recommended to keep the station instruments properly calibrated and maintained.  
111 The assessment of long-term data by comparing to local measurements could help in  
112 terms of uncertainty quantification and mitigating the financing risk of the project

113 (Armansperg et al., 2015; Fernández-Peruchena et al., 2018; Fernández Peruchena et  
114 al., 2016; Guerreiro et al., 2016; Hirsch et al., 2017; Meyer and Schwandt, 2017; Polo et  
115 al., 2017, 2016a; Richter et al., 2015). Moreover, a reasonable period of ground  
116 measurements (usually a year) can be used to remove bias, and thus correct and  
117 improve the long-term solar radiation time series by different techniques. These  
118 techniques aim to find a relationship between the ground and modeled data that can  
119 be extrapolated to the past, as a means for minimizing the statistical deviations. This  
120 process of calibration or correction of modeled data by including observational data  
121 has been used in the retrievals of other meteorological variables (wind velocity,  
122 precipitation, etc.). In the field of energy meteorology, such correction procedures  
123 have been frequently termed *site adaptation* techniques (Polo et al., 2016b). Several  
124 example techniques that have been applied to improve the goodness of solar radiation  
125 time series can be found in the recent literature (Frank et al., 2018; Mazonra Aguiar et  
126 al., 2019; Perez et al., 2010; Polo et al., 2015; Tahir et al., 2020).

127

128 In the framework of the Task 16 of IEA-PVPS (<http://www.iea-pvps.org/index.php?id=389>)  
129 and Task V of IEA-SolarPACES entitled “Solar Resource for High Penetration and Large  
130 Scale Applications”, several activities are being addressed in benchmarking, models  
131 assessment and improving knowledge of modeling solar radiation components.  
132 Improvement in measuring protocols, gap filling, and quality check of ground data and  
133 benchmarking of models are, among others, activities focused on improving the  
134 bankability of solar radiation products. In this context, benchmarking and reviewing of  
135 site-adaptation techniques for solar resource data are stated as activities of interest  
136 (Remund et al., 2017). Under this framework, several task participants are developing  
137 different techniques and procedures for improving and correcting the modeled  
138 datasets, for various satellite-derived and reanalysis datasets, in order to have a  
139 sample of modeled solar radiation data that can typify the different types of  
140 uncertainties.

141

142 A first benchmarking exercise has been developed by four teams of scientists, and its  
143 methodology and results are reported here. Each team has implemented one or  
144 several site adaptation techniques, according to their previous experience and skills.  
145 All these methodologies have been applied in a blind exercise to 10 different datasets  
146 (consisted of pairs of ground and model sets of data of the solar irradiance  
147 components: GHI, DNI and DHI).

148

149 For the present needs, a blind exercise is justified to protect some of the techniques  
150 that are, or could be become, commercial. This study aims at performing a pure  
151 statistical exercise to explore the capability of a given technique to improve a dataset  
152 using a small part of the observations. Therefore ground and model datasets, and  
153 techniques, are selected following these simple rules: covering quite different climates,

154 using mostly free and open-source modeled and ground data, and selecting those site  
155 adaptation techniques with enough details in the literature for easy implementation.  
156 This paper acts as a report for those findings.

157

## 158 **2. Description of the methodologies and approaches**

159

160 Different methodologies have been tested in this work for site adaptation of solar  
161 radiation data. Some of them originate from other subdomain of meteorology (Piani et  
162 al., 2010; Wilcke et al., 2013). This section provides a general description of the  
163 fundamentals of those methodologies considered in this work. It is emphasized that  
164 more site adaptation techniques do exist, and some of them were described in Polo et  
165 al. 2016; hence, the present contribution should not be considered exhaustive. The  
166 procedures for using these techniques can be applied to either the entire dataset, or  
167 subsets of data that are divided according to solar elevation or sky classification, for  
168 instance. In order to emulate a realistic situation in resource assessment for solar  
169 projects, each site-adaptation procedure has been carried out using data from the  
170 latest year available at each site, and each adapted series has been compared with  
171 measured data spanning the entire history of that site.

172

### 173 **2.1 Linear regression bias removal**

174

175 The bias removal using a linear regression model aims at finding a linear relationship  
176 between the measured and modeled data, which often can result in an improved  
177 coefficient of determination of the pair of random variables. This simple methodology  
178 is quite commonly used to correct satellite-derived solar radiation data, showing good  
179 results in presence of large seasonal bias (Mazorra Aguiar et al., 2019; Polo et al.,  
180 2016b, 2015). Linear least squares fitting is performed between the modeled data ( $x_m$ )  
181 and observations ( $x_o$ ) over a selected period of time (e.g., one year) to obtain the  
182 slope ( $a$ ) and the y-intercept ( $b$ ). The bias-removal procedure for the fitting data can  
183 be expressed using the following equation:

184

$$185 \quad y = x_m - [(a-1) x_o + b]. \quad (1)$$

186

187 Such expression of  $y$  and  $x_m$  results in a linear function  $f$  that can be used to transform  
188 all the historical modeled data into new corrected data,  $y_c$ .

189

$$190 \quad y_c = f(x_m), \quad (2)$$

191

192 where  $f$  represents the linear function resulting from fitting the corrected  $y_c$  values  
193 versus the original  $y$ . This procedure has similarities with the Measured-Related-

194 Predict (MCP) methods (Carta et al., 2013). In the context of this work this method will  
195 be called LIN-FIT for better comparison with the other methodologies used here.

196

## 197 2.2 Quantile mapping (QM)

198

199 The quantile mapping (QM) technique has been employed in climate modeling and  
200 meteorology for correcting the distribution of a modeled parameter by comparing it  
201 against the empirical distribution of the observations (Déqué et al., 2007; Ines and  
202 Hansen, 2006). The approach seeks to transform the data to a probability domain  
203 (quantiles) and applies the inverse transformation using the cumulative distribution  
204 function (CDF) of the observational data to obtain the corrected data (Déqué et al.,  
205 2007),

206

$$207 \quad y_c = \text{CDF}_o^{-1}[\text{CDF}_m(x_m)], \quad (3)$$

208

209 where  $\text{CDF}_o$  and  $\text{CDF}_m$  are the cumulative distribution functions of the observed and  
210 modeled data, respectively.

211 The quantiles of modeled and observed data can be computed by the full empirical  
212 non-parametric distribution or by a fitted theoretical parametric distribution  
213 (Feigenwinter et al., 2018; Piani et al., 2010; Themeßl et al., 2012).

214

## 215 2.3 Quantile delta mapping (QDM)

216

217 The quantile delta mapping (QDM) bias-correction method is an extension of the  
218 conventional QM technique (Cannon, 2018; Cannon et al., 2015). The algorithm  
219 preserves the model-projected relative changes in quantiles, and additionally, corrects  
220 the systematic quantile biases of the modeled data with respect to the observed  
221 values. The bias-adjustment of the modeled values for the reference period is the  
222 same as the traditional QM technique. With respect to the target variable, two  
223 corrections are applied (additive and multiplicative):

224

$$225 \quad y_c = x_m + \text{CDF}_o^{-1}[\text{CDF}_m(x_m)] - \text{CDF}_m^{-1}[\text{CDF}_m(x_m)], \quad (4)$$

$$226 \quad y_c = x_m \frac{\text{CDF}_o^{-1}[\text{CDF}_m(x_m)]}{\text{CDF}_m^{-1}[\text{CDF}_m(x_m)]}.$$

227

228           2.4 Cumulative distribution function-transform (CDF-T)

229

230   The CDF-T method performs QM based on the CDFs over the future period, thus,  
231   allowing the CDF to change with respect to the reference period. It provides an  
232   extension of the traditional QM method since the QM technique only transforms the  
233   modeled values of the future period onto the CDF of the reference period  
234   (Michelangeli et al., 2009).

235

236

237           2.5 Kernel density distribution mapping (KDM)

238

239   Kernel density distribution mapping (KDM) method uses a similar logic as QM, at least  
240   algorithmically. In general, QM enables the bias-adjustment by transforming the  
241   modeled values into quantiles, and then projecting them into data values in terms of  
242   the quantile function (inverse CDF) of the observations (McGinnis et al., 2015). In KDM  
243   the CDF and the CDF<sup>-1</sup> functions are expressed in terms of the kernel density estimator. The  
244   probability density functions (PDF) of the modeled and the observed values are estimated non-  
245   parametrically using kernel density estimation assuming a Gaussian kernel (Izenman, 2016).  
246   Two slightly different versions of KDM have been used in this work. KDM-T and KDM-CS refer  
247   to the application of the technique to the whole dataset and to subsets according to sky  
248   conditions (clear or non-clear), respectively. KDMR is just KDM with an optimal bandwidth  
249   algorithm.

250

251           2.6 Site-specific multiple regression (SIM)

252   This method is based on the multi-model inference (also known as ensemble) of multiple linear  
253   regression models, through computing, comparing, and ranking an exhaustive list of models.  
254   For the local adaptation of GHI, an exhaustive screening of the selected exogenous variables is  
255   carried out, followed by a selection of a best model as per the Akaike information criterion  
256   (AIC). The model is constructed through both the selected variables and their interactions; the  
257   exogenous variables include clearness index of modeled GHI series ( $K_t$ , the ratio of GHI to top-  
258   of-atmosphere solar irradiance on the same plane); relative air mass ( $m$ ); modeled clear-sky  
259   index ( $K_c$ , the ratio between modeled GHI and its corresponding value under clear-sky  
260   conditions); and solar elevation angle. The clear-sky model used in this method is McClear  
261   (Lefèvre et al., 2013), available through the Copernicus Atmosphere Monitoring Service  
262   (CAMS, <http://www.soda-pro.com/web-services/radiation/cams-mcclear> ).

263   The methodology for the local adaptation of DNI is based on the previous adaptation of the  
264   diffuse horizontal irradiance (DHI), because the ratio DHI to GHI ( $K$ , diffuse fraction) is known  
265   to be reliably predictable from the following parameters (and their combinations):  $m$ ,  $K_c$ , solar  
266   elevation, and a fourth-order polynomial of  $Kt_m$ . Finally, DNI is calculated from both locally  
267   adapted GHI and DHI by the closure equation, assuring the accomplishment of the  
268   fundamental relations between these solar radiation components. Finally, the procedure is  
269   applied separately for clear-sky and non-clear-sky days.

## 270 2.7 Sequential regressive-quantile mapping procedure (SIMEQ)

271 This method is a sequential application of two procedures of different nature. Firstly, the SIM  
272 technique (described in the preceding subsection, 2.6) is applied, which is based on the  
273 multimodel inference of multiple linear regression models. Secondly, a bias correction based  
274 on empirical quantile mapping (eQM) is applied on both GHI and DNI adapted series. This  
275 method consists in calibrating the simulated CDF by adding to the observed quantiles both the  
276 mean delta change and the individual delta changes in the corresponding quantiles. Finally,  
277 DHI is calculated from the locally adapted GHI and DNI, through the closure equation, thus  
278 satisfying the fundamental relations between these solar radiation components.

279 The first procedure (i.e., the SIM method) can considerably reduce both the dispersion and the  
280 deviation in CDF of the adapted solar irradiance series, with respect to the modeled ones. The  
281 application of the second procedure (eQM) to the mentioned adapted series significantly  
282 reduces the deviation in CDF, while maintaining or reducing the values of the dispersion  
283 statistical indicators. Similar to the case of the SIM technique, this procedure is applied  
284 separately to clear and non-clear-sky days.

285

## 286 2.8 Regressions using subsets of data

287 Specific regressions and fitting techniques can be also applied to subsets of data as a  
288 site adaptation procedure. In this paper a methodology is used for correcting only GHI  
289 where subsets of ground and modeled data are first classified into different ranges of  
290 solar zenith angles and clear-sky index,  $K_{cs}$  (the ratio between the modeled GHI and its  
291 corresponding value under clear-sky conditions). Solar zenith angles are divided into 5  
292 groups in the range of 0-75° with intervals of 15°, whereas  $K_{cs}$  is divided into two  
293 groups, namely lower and greater than 0.55. For each combination of groups (10  
294 combinations in total), a pair of third-degree polynomial regressions are applied to the  
295 last year of modeled and ground data - one for GHI and the other one for  $K_{cs}$ .  
296 Moreover, two additional regressions (again one for GHI and one for  $K_{cs}$ ) are  
297 calculated from samples of the entire year (solar zenith angle between 0-75° and  $K_{cs}$   
298 between 0 and 1). This makes a total of 22 regressions. The one that minimizes the  
299 relative bias is picked for this particular subsample.

## 300 3. Ground and modeled datasets

301 In order to benchmark the different site adaptation techniques, sites are selected from  
302 locations under different climates, and covered by different networks of ground stations. In  
303 addition, different types of modeled data (i.e., satellite-derived and reanalysis) are used. Most  
304 of these data belong to different satellite-derived datasets, estimated using different methods,  
305 and issued by various providers. Reanalysis data, on the other hand, cover two high-latitude  
306 sites, where satellite images do not resolve. Table 1 summarizes the metadata of the selected  
307 sites, which are drawn on the world map together with their climatic types in Figure 1. In this  
308 regard, the datasets herein used belong to modeled data with very different uncertainties



309 corresponding to two different reanalyses, several satellite models with different approaches  
 310 regarding the clear-sky transmittance, atmospheric information (aerosol optical depth or  
 311 turbidity, water vapor and other components) and satellite imagery (different satellite  
 312 platforms). Each dataset contains both the modeled and measured hourly values of the three  
 313 basic solar radiation components (GHI, DNI and DHI). In addition, some, but not all, BSRN-  
 314 recommended quality checks for ground data are performed (Long and Dutton, 2004), for both  
 315 ground and model data. The reason is to allow the assessment of site adaptation methods as a  
 316 “blind” statistical tool attempting to fit different model data to observational ones.

317 Table 1. Summary of sites with pair ground-model datasets for benchmarking

Site (code)	Latitude (°N)	Longitude (°E)	Elevation (m)	Climate	Period	Model type
<b>Alice Springs (ASP)</b>	-23.79	133.88	547	Hot desert, arid	2007-2013	Satellite
<b>Boulder (BOU)</b>	40.12	-105.23	1689	Cold semi-arid	2009-2015	Satellite
<b>Tateno (TAT)</b>	36.05	140.12	25	humid subtropical	2009-2015	Satellite
<b>Tamanrasset (TAM)</b>	22.79	5.52	1385	Hot desert, arid	2007-2011	Satellite
<b>Carpentras (CAR)</b>	44.08	5.05	100	Mediterranean	2007-2013	Satellite
<b>Burns (BRN)</b>	43.52	-119.02	1271	Cold semi-arid	2007-2013	Satellite
<b>Kiruna (KIR)</b>	67.48	20.41	424	subarctic	2008-2014	Reanalysis
<b>Norrköping (NRK)</b>	58.58	16.14	53	humid continental	2008-2014	Reanalysis
<b>Visby (VIS)</b>	57.67	18.34	49	oceanic	2008-2014	Satellite
<b>Sede Boqer</b>	30.86	34.77	500	Hot desert, arid	2006-2011	Satellite

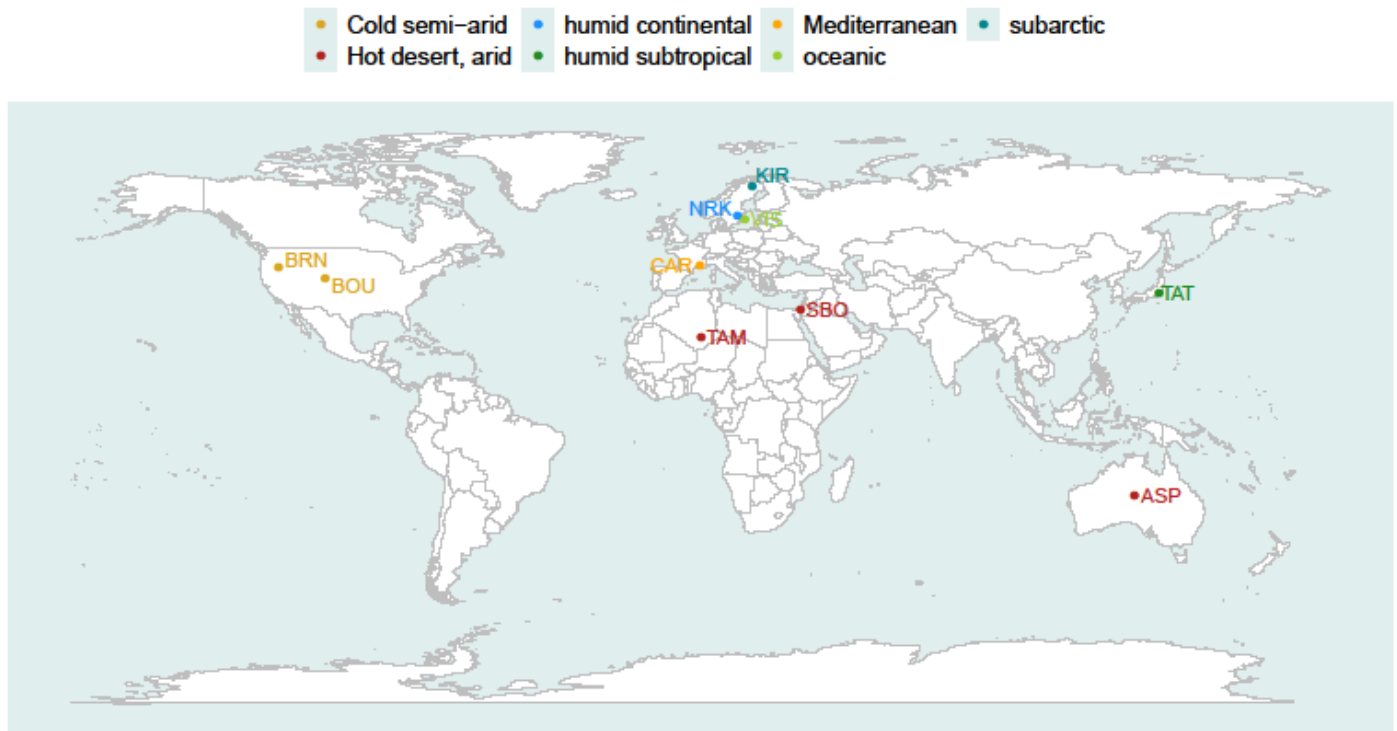
318

319

#### 320 4. Deviations of the model datasets

321 The evaluation approach for the modeled datasets is described before presenting the  
 322 results of the different site adaptation techniques. For assessment of model and site  
 323 adaptation performance, three metrics are selected: mean bias deviation (MBD), root  
 324 mean square deviation (RMSD) and Kolmogorov-Smirnov integral (KSI). The first two  
 325 accuracy measures indicate bias and dispersion, whereas the third informs the  
 326 similitude of CDFs of modeled and measured data (Gueymard, 2014). Table 2 shows  
 327 the statistical metrics expressed in percent of all the modeled datasets (i.e. the original  
 328 uncorrected datasets as delivered by the different models used) for the three  
 329 components. Large ranges of bias, dispersion and similitude of distribution functions in  
 330 the model dataset can be observed as a consequence of taking both the site  
 331 characteristics and the approaches into account in the modeling. This is a good  
 332 outcome from the study since the scope of this work is not the performance of models

333 retrieving solar radiation data but the capability of statistical methods to correct any  
334 model according to short-term observational values.



335

336 Figure 1. Sites selected for benchmarking site adaptation methods.

337

### 338 5. Site adaptation assessment results

339 Different procedures for site adaptation (up to 12) based on the previously described  
340 techniques (in Section 2) were used by four different teams in their attempt to  
341 generate corrected or improved values of the 10 datasets. Table 3 summarizes the  
342 characteristics of each procedure and details the team that employed each procedure.  
343 In all cases, the most recent year of ground data was used to train the model whereas  
344 the adaptation was applied to the whole period of the modeled dataset under  
345 scrutiny. It should be noted that eQM-CS and KDM-CS methods differ from other  
346 quantile mapping methodologies, since they are applied separately to the two subsets

347 of modeled data that had been obtained for each sky condition (clear or non clear-  
348 sky). Therefore, prior to the use of those methods a selection of model data was done  
349 using an algorithm for automatic detection of clear-sky instants. In the case of eQM-CS  
350 and KDM-CS, the clear-sky detection is done using a method proposed by Gueymard  
351 2013. The procedure requires DNI observations and concomitant DNI estimations  
352 under clear-sky conditions based on reliable aerosol optical depth (AOD) data. There is  
353 no perfect algorithm for a posteriori clear-sky identification in solar irradiance time  
354 series since any method may be affected by various sources of error, including  
355 inaccuracies in the input required. For instance, the computation of clear-sky  
356 components need of very accurate information of AOD and Precipitable water at least)  
357 (Gueymard, 2013; Gueymard et al., 2019). A very promising new model has been  
358 recently proposed in the literature for 1-min data (Bright et al., 2020). However the  
359 specific algorithm used in this work points the potential benefits of an accurate  
360 separation of clear and non clear-sky instants in site adaptation methodologies.

361  
362  
363  
364

Table 2. Statistical metrics for the performance of uncorrected modeled datasets.

Site	GHI (%)			DNI (%)			DHI (%)		
	MBD	RMSD	KSI	MBD	RMSD	KSI	MBD	RMSD	KSI
<b>Alice Springs</b>	0.0	12.2	49.1	-1.1	20.1	203.7	3.2	47.1	127.1
<b>Boulder</b>	0.1	25.8	92.3	-6.1	49.9	102.6	9.7	50.6	99.3
<b>Tateno</b>	-3.3	18.3	46.9	-5.5	32.8	81.6	-1.3	31.2	117.6
<b>Tamanrasset</b>	-5.9	16.8	75.4	-12.7	38.8	223.7	9.8	51.7	206.8
<b>Carpentras</b>	2.6	17.4	50.1	3.6	31.5	64.7	3.7	42.0	144.9
<b>Burns</b>	-1.0	26.9	78.6	5.8	37.7	109.8	-9.6	60.1	247.6
<b>Kiruna</b>	106.9	258.3	31.1	39.4	179.7	23.3	26.8	141.6	37.7
<b>Norrkoping</b>	36.6	172.2	21.6	-18.6	118.5	18.7	33.9	141.7	43.4
<b>Visby</b>	33.1	170.2	28.6	-11.3	123.3	21.2	25.5	138.0	52.5
<b>Sede Boqer</b>	-3.9	33.7	75.1	-15.3	42.4	207.7	19.2	59.6	334.1

365  
366  
367  
368  
369

Table 3. Summary of site adaptation techniques and procedures.

Name	Type	Components	Observations	Team
<b>eQM-T</b>	Quantile Mapping	GHI,DNI,DHI	Empirical CDF	Team 1
<b>eQM-CS</b>	Quantile Mapping	GHI,DNI,DHI	Empirical CDF, separately to clear and non-clear-sky data	Team 1
<b>KDM-T</b>	Quantile Mapping	GHI,DNI,DHI	Kernel Density Distribution Mapping, limiting the maximum irradiance in the CDF to 5% over maximum observed	Team 1
<b>KDM-CS</b>	Quantile Mapping	GHI,DNI,DHI	Same as before but separately to clear and non-clear-sky data	Team 1
<b>LIN-FIT</b>	Regression	GHI,DNI,DHI	Simple linear fit	Team 2
<b>CDF-T</b>	Quantile Mapping	GHI,DNI,DHI	As described in section 2.4	Team 2

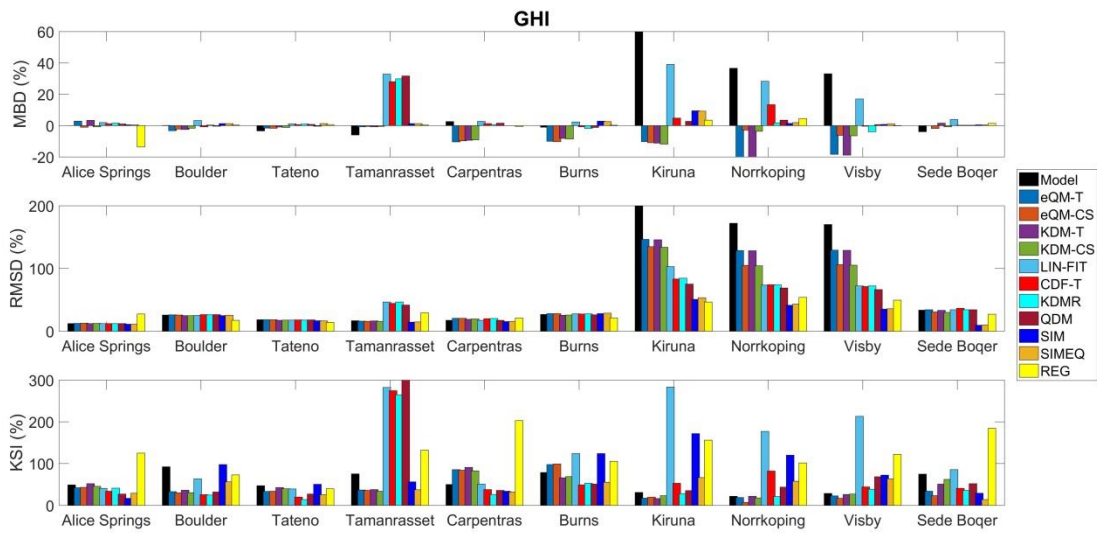
<b>KDMR</b>	Quantile Mapping	GHI,DNI,DHI	Kernel Density Distribution Mapping with optimal bandwidth	Team 2
<b>QDM</b>	Quantile Mapping	GHI,DNI,DHI	As described in section 2.3	Team 2
<b>SIM</b>	Multiple Regression	GHI,DNI,DHI	As described in section 2.6	Team 3
<b>SIMEQ</b>	Sequential	GHI,DNI,DHI	As described in section 2.7	Team 3
<b>REG</b>	Regression	GHI	As described in section 2.8	Team 4

370

371

372 Figures 2, 3 and 4 show the statistical metrics of the performance of the eight site  
 373 adaptation methods for the GHI, DNI and DHI components, respectively. The first  
 374 entry, referred to as model, indicates the original uncorrected modeled data in order  
 375 to allow proper comparison and to illustrate the relative improvement in performance  
 376 generated by each site adaptation method.

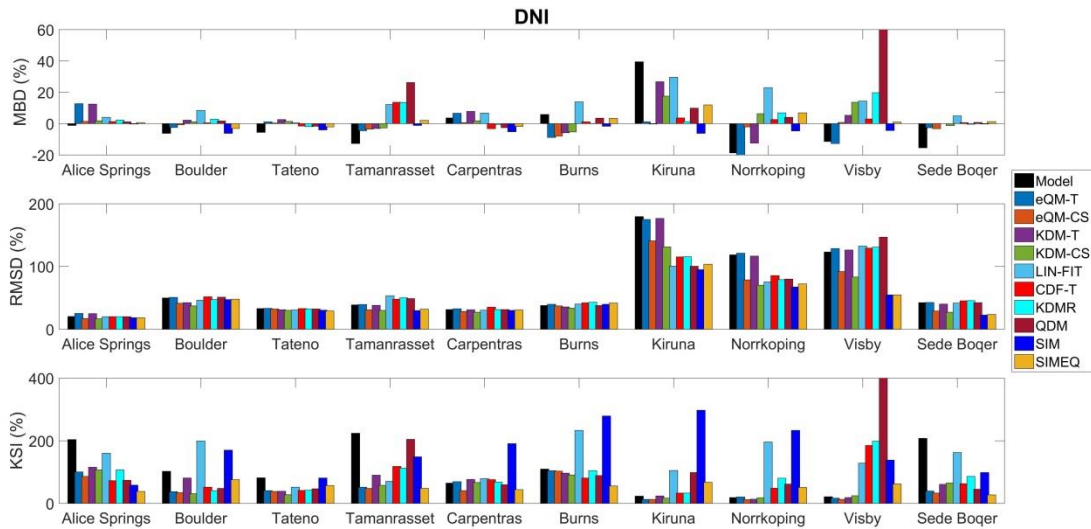
377



378

379 Figure 2. Statistical metrics for benchmarking of site adaptation applied to GHI.

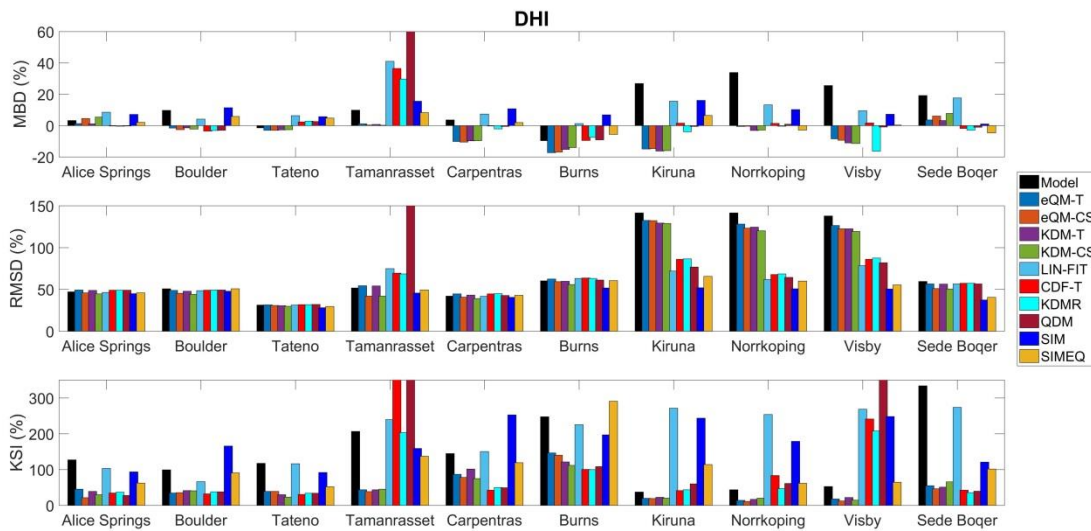
380



381

382 Figure 3. Statistical metrics for benchmarking of site adaptation applied to DNI.

383



384

385 Figure 4. Statistical metrics for benchmarking of site adaptation applied to DHI.

386 The benchmarking results for GHI show that bias is not successfully removed in all  
 387 cases. In particular, modeled datasets having an originally low bias (< 1%) site do not  
 388 benefit from any improvement, with the exception of some QM-based (CDF-T, KDMR,  
 389 QDM) and multiple regression based (SIM, SIMEQ) methods. However, in the case of  
 390 modeled data with significant bias (> 30%), most techniques generally result in MBD  
 391 improvement compared to unprocessed model data resulting in a much lower MBD  
 392 (<10%) for most of them, and even in negligible bias (<1%) in the case of KDMR.

393

394 RMSD is very slightly improved by most techniques, except in the case of modeled  
395 datasets corresponding to the three sites (Kiruna, Norrköping, and Visby) at very high  
396 latitude ( $>55^\circ$ ), where the original modeled data are affected by substantial  
397 uncertainty (Table 2), and where the site adaptation techniques induce a significant  
398 decrease in random errors. At those sites with the lowest RMSD values ( $< 20\%$ ), only  
399 those methods based on multiple regression (SIM, SIMEQ) achieved RMSD reduction  
400 (from 16.2% to 14.5%).

401

402 In the case of DNI, most of the methods are able to achieve significant improvement  
403 over the highly negatively biased modeled data (with typical MBD of  $\sim 15\%$ ), even  
404 bringing down the MBD to below 3% with some of them (eQM-CS, KDM-T, SIM and  
405 SIMEQ). The highly positively biased site (Kiruna, MBD = 39.5%) is satisfactorily  
406 corrected by some methods, among which eQM-T and eQM-CS should be highlighted.  
407 On the other hand, sites with moderate MBD (BOU and TAT, negatively bias at  $\sim 5.8\%$ ,  
408 and CAR and BRN, positively bias at  $\sim 4.8\%$ ) are satisfactorily corrected by most  
409 methods. Conversely, RMSD is more significantly improved by only some techniques.  
410 In particular, sites with high RMSD (KIR, NRK and VIS, with RMSD  $\sim 140\%$ ) are on  
411 average improved by all methods, among which SIM and SIMEQ should be highlighted  
412 because they reduce RMSD by half. At all other sites (typical RMSD  $\sim 36\%$ ), only some  
413 methods based both on QM (eQM-CS, KDM-T, KDM-CS) and multiple regression (SIM  
414 and SIMEQ) achieve improvements.

415

416 For the case of DHI, the situation at high-bias sites (MBD  $> 20\%$ ) is generally improved  
417 by the site adaptation techniques, whereas very different results are obtained at low-  
418 bias sites. Performance improvement in terms of RMSD is mainly observed for a few  
419 datasets wherever the initial bias is large.

420

421 On the other hand, there are some methods that eventually show a characteristic bad  
422 performance not observed at other sites. Thus, LIN-FIT, CDF-T, KDMR and QDM  
423 showed slightly or remarkable improvement in GHI and DHI except at Tamanrasset  
424 site. This particular behavior cannot be attributed to a particular site adaptation  
425 method, so that other potential causes would need to be investigated, such as  
426 subjective user interventions or impacts of the specific training year selected for those  
427 methods.

428

429 KSI is a metric difficult to evaluate in general. Nevertheless, a general better  
430 performance can be observed in the three components by all QM-based methods as  
431 well as in SIMEQ (which uses an eQM procedure). Exceptions to this observation for  
432 some methods (CDF-T, KDM-R and QDM) may be found for Tamanrasset (due probably  
433 to unknown reasons beyond the methodology) and at very high-latitude sites.  
434 Obtaining any improvement at the three high-latitude sites is very challenging because

435 their measured global irradiance can be positive at zero or negative sun elevation  
 436 angles, and because the models selected for these sites were apparently highly  
 437 uncertain.

438

439 Condensing the benchmarking and comparisons results in one unique and proper  
 440 parameter might be questionable; however, in order to illustrate the results a unique  
 441 metric called combined performance Index (CPI) can be used here (Gueymard, 2014).  
 442 CPI is defined as a weighted sum of several metrics to combine information on the  
 443 dispersion and on the distribution function similitude as well. That is,

444

$$445 \quad \quad \quad CPI = (KSI + OVER + 2 RMSE)/4. \quad (5)$$

446

447 Tables 4, 5 and 6 show the performance of the different site adaptation techniques for  
 448 GHI, DNI and DHI, respectively, in terms of CPI (in percentage). In these tables, the row  
 449 denoted as Raw Model and highlighted in bold refers to the original uncorrected  
 450 model dataset. According to these results most methods resulted in improvement of  
 451 the model datasets. There are, nevertheless, exceptions, such as the LIN-FIT method,  
 452 that performs worse at Burns and at high-latitude sites. Despite the absence of any  
 453 universal rule in the results, in several situations benefits can be obtained by  
 454 separating the data into two subsets (clear and non-clear sky). In addition, the  
 455 sequential use of methods, as occurs in the SIMEQ methodology, produces better  
 456 performance. Quantile mapping based methodologies, in general, tend also to reduce  
 457 the uncertainty.

458

459

460 Table 4. CPI (%) for GHI benchmarking results.

461

462

	ASP	BOU	TAT	TAM	CAR	BRN	KIR	NRK	VIS	SBO	P50*
<b>Raw Model</b>	<b>25.5</b>	<b>54.0</b>	<b>23.7</b>	<b>39.7</b>	<b>25.2</b>	<b>46.0</b>	<b>138.1</b>	<b>91.5</b>	<b>92.3</b>	<b>45.6</b>	<b>45.8</b>
eQM-T	18.6	21.4	17.5	20.7	45.0	52.6	77.7	70.1	71.6	30.6	<b>37.8</b>
eQM-CS	19.3	20.4	17.7	20.3	46.3	52.9	72.3	54.4	57.4	22.7	<b>34.5</b>
KDM-T	24.5	23.4	21.2	20.9	48.2	36.7	78.1	70.8	72.6	36.6	<b>36.7</b>
KDM-CS	22.0	20.0	20.6	17.6	40.3	37.5	73.8	56.7	59.5	39.6	<b>38.6</b>
LIN-FIT	20.5	42.7	20.5	163.7	24.5	67.8	190.3	122.7	141.5	53.3	<b>60.6</b>
CDF-T	14.7	19.6	13.9	158.3	21.4	27.3	60.2	72.5	46.6	32.7	<b>30.0</b>
KDMR	20.6	19.2	12.5	155.4	16.7	33.8	51.6	43.3	49.2	29.5	<b>31.7</b>
QDM	12.9	21.2	15.8	177.8	17.6	30.1	48.4	51.2	63.8	34.9	<b>32.5</b>
SIM	9.8	55.2	27.3	25.1	17.8	70.2	109.6	75.9	49.4	12.1	<b>38.4</b>
SIMEQ	12.9	34.1	15.8	16.8	15.9	33.8	51.1	46.0	42.8	8.4	<b>25.3</b>
REG	71.5	37.6	21.0	76.8	109.4	59.2	97.5	71.5	79.1	101.5	<b>74.2</b>

463 \*Median of CPI for all sites

464  
465  
466  
467

Table 5. CPI (%) for DNI benchmarking results.

	<b>ASP</b>	<b>BOU</b>	<b>TAT</b>	<b>TAM</b>	<b>CAR</b>	<b>BRN</b>	<b>KIR</b>	<b>NRK</b>	<b>VIS</b>	<b>SBO</b>	<b>P50*</b>
<b>Raw Model</b>	<b>109.3</b>	<b>70.3</b>	<b>53.5</b>	<b>129.0</b>	<b>37.8</b>	<b>69.0</b>	<b>97.4</b>	<b>64.0</b>	<b>67.0</b>	<b>121.2</b>	<b>81.9</b>
<b>eQM-T</b>	58.3	36.4	28.3	32.8	42.3	62.5	90.8	67.1	68.5	33.6	<b>52.1</b>
<b>eQM-CS</b>	43.1	30.5	27.3	29.4	24.5	63.6	73.6	42.4	49.2	24.7	<b>40.8</b>
<b>KDM-T</b>	64.0	56.7	26.1	57.9	44.1	58.2	95.8	61.7	68.9	44.8	<b>57.8</b>
<b>KDM-CS</b>	56.7	30.7	22.0	34.8	40.2	53.4	71.1	39.6	49.7	36.1	<b>43.4</b>
<b>LIN-FIT</b>	80.7	118.9	31.2	54.5	50.2	131.5	93.8	129.0	123.4	94.6	<b>90.8</b>
<b>CDF-T</b>	40.0	40.0	26.9	76.5	47.1	49.6	65.9	56.6	153.5	48.1	<b>60.4</b>
<b>KDMR</b>	56.7	35.7	28.6	76.9	43.8	63.2	66.1	69.7	163.0	60.9	<b>66.5</b>
<b>QDM</b>	39.1	40.0	28.0	121.8	39.8	57.2	93.5	61.0	370.4	37.4	<b>88.8</b>
<b>SIM</b>	31.5	103.1	43.8	82.1	106.2	157.3	193.1	147.7	88.3	53.0	<b>100.6</b>
<b>SIMEQ</b>	21.4	54.5	35.5	30.6	31.0	41.0	78.7	53.5	49.5	18.5	<b>41.4</b>

468 \*Median of CPI for all sites

469  
470  
471  
472  
473  
474

Table 6. CPI for DHI benchmarking results.

	<b>ASP</b>	<b>BOU</b>	<b>TAT</b>	<b>TAM</b>	<b>CAR</b>	<b>BRN</b>	<b>KIR</b>	<b>NRK</b>	<b>VIS</b>	<b>SBO</b>	<b>P50*</b>
<b>Raw Model</b>	<b>83.0</b>	<b>68.2</b>	<b>69.1</b>	<b>123.8</b>	<b>89.7</b>	<b>150.8</b>	<b>83.4</b>	<b>84.8</b>	<b>86.2</b>	<b>193.8</b>	<b>103.3</b>
<b>eQM-T</b>	43.1	37.9	27.6	41.9	62.1	99.4	71.2	67.5	67.9	54.2	<b>57.3</b>
<b>eQM-CS</b>	29.4	36.0	27.1	34.4	55.5	94.9	71.0	64.6	64.4	43.4	<b>52.1</b>
<b>KDM-T</b>	39.3	41.3	22.8	42.6	68.8	82.5	70.3	66.5	67.9	52.1	<b>55.4</b>
<b>KDM-CS</b>	31.4	38.0	20.8	40.8	53.0	77.8	69.5	65.2	63.4	52.7	<b>51.3</b>
<b>LIN-FIT</b>	71.8	49.8	70.5	155.2	93.9	138.3	170.6	153.7	167.9	162.2	<b>123.4</b>
<b>CDF-T</b>	34.8	34.3	23.7	226.0	36.0	75.1	56.6	71.0	160.4	46.3	<b>76.4</b>
<b>KDMR</b>	36.5	37.4	28.3	133.2	43.3	74.4	58.0	51.5	142.7	43.0	<b>64.8</b>
<b>QDM</b>	31.5	37.4	26.5	415.9	40.7	81.3	63.3	59.0	214.9	45.5	<b>101.6</b>
<b>SIM</b>	63.4	103.8	53.6	96.8	141.6	119.4	144.3	110.7	144.1	77.3	<b>105.5</b>
<b>SIMEQ</b>	49.3	64.3	32.1	83.8	75.6	171.2	83.6	55.5	52.5	69.1	<b>73.7</b>

475 \*Median of CPI for all sites

476  
477

## 6. Sensitivity analysis

479 In addition to the benchmarking exercise, where the last complete year of ground  
480 measurements was used for training the improvement method, a sensitivity analysis



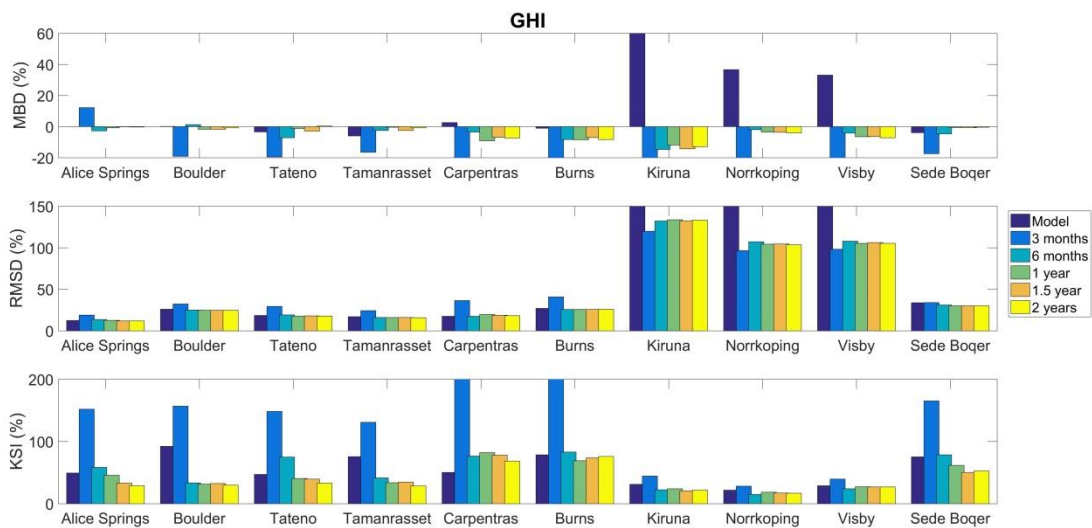
481 on the training period was performed. This analysis was intended to determining the  
 482 minimum period of time that should be used in the ground database for proper  
 483 training. The sensitivity analysis has consisted in performing site adaptation to the 10  
 484 datasets of table 2 using the eQM-CS method with training periods of 3 months, 6  
 485 months, 1 year, 1.5 year and 2 years.

486

487 Figures 5 and 6 show the main statistical performance metrics for GHI and DNI (very  
 488 similar results were found for DHI) compared to the uncorrected dataset referred to as  
 489 model. It can be observed that a period of 3 months is insufficient to obtain significant  
 490 improvement in most cases. Remarkably, such a short period tends to increase the KSI  
 491 significantly, indicating that corrected data resulted in a worse similitude with the  
 492 distribution function than the uncorrected data. For most of the cases, the sensitivity  
 493 analysis indicates that 1-2 years of quality ground measurements are necessary to  
 494 result in a general improvement of the solar radiation adapted data.

495

496

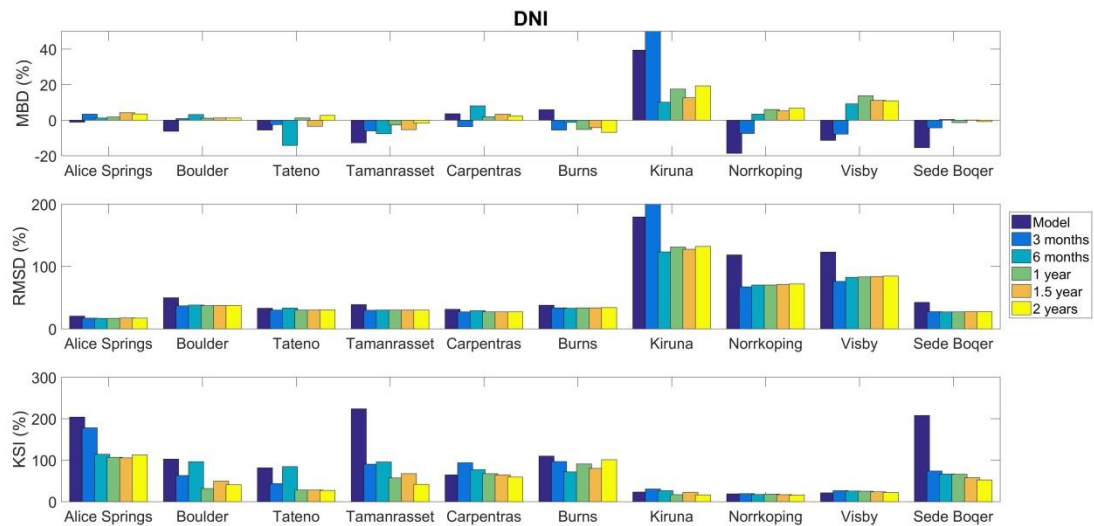


497

498

499 Figure 5. Sensitivity of GHI performance to the training period duration.

500



501

502

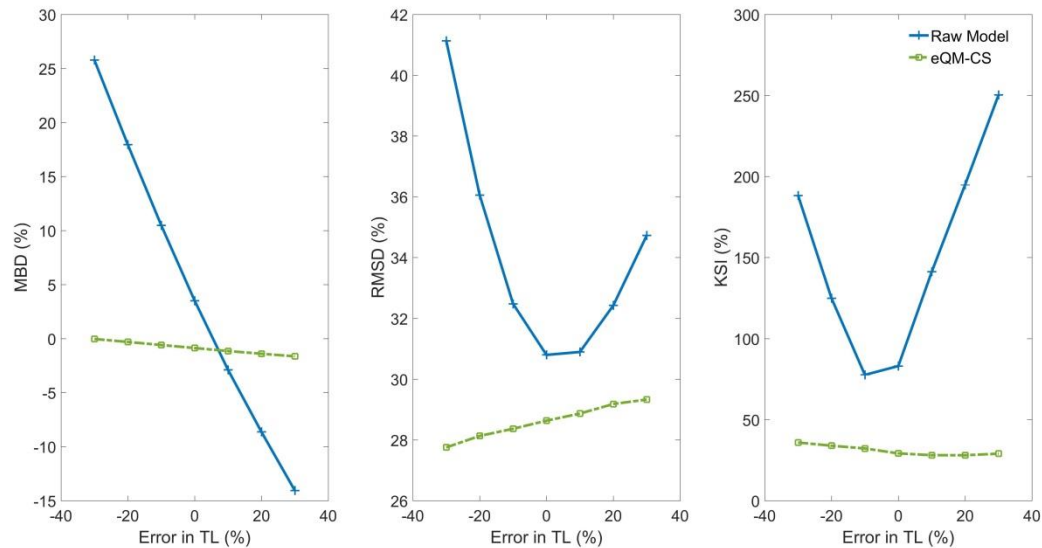
503 Figure 6. Sensitivity of DNI performance to the training period duration.

504

505 The sensitivity to a very large uncertainty in aerosol data (AOD, most importantly) or in  
 506 the abundance of other atmospheric constituents in general can be also of interest,  
 507 particularly for modeling DNI, which is the component strongly influenced by  
 508 atmospheric aerosols and water vapor content in the atmosphere (Gueymard, 2012;  
 509 Polo and Estalayo, 2015). The sensitivity analysis has been done by firstly generating  
 510 satellite-derived DNI datasets for Carpentras, assuming different values (in terms of  
 511 uncertainty in the atmospheric input) for the corresponding Linke turbidity factor. The  
 512 latter's original estimated value at that site was adjusted in the range -30% to 30%.  
 513 Assuming that the original TL value is perfectly true then the deviations can be  
 514 considered as errors in the TL determination. Thus, regardless of the uncertainty in the  
 515 original Linke turbidity factor, this sensitivity offers an assessment of the capability of  
 516 site adaptation methods to correct situations with large overestimations or  
 517 underestimations in atmospheric attenuating constituents. Here, the eQM-CS  
 518 methodology was used for adapting or improving all the sensitivity cases. Figure 7  
 519 shows the sensitivity analysis results in terms of MBD, RMSD and KSI as a function of  
 520 the assumed error in the TL value used as input to the satellite model. In this case a  
 521 significant reduction in bias, dispersion and KSI is achieved by the correction method,  
 522 even for very large over- and under-estimation of the atmospheric turbidity. Likewise,  
 523 removal of substantial part of bias observed in DNI datasets with inaccurate aerosol  
 524 information has been also reported in studies with other correction techniques  
 525 (Gueymard, 2011; Gueymard et al., 2012).

526

527



528  
529

530 Figure 6. Sensitivity to the Linke turbidity uncertainty. Performance metrics of DNI for  
531 both the raw model and after correction with the eQM-CS method are shown.

532 **7. Conclusion**

533 Site adaptation of model-derived solar radiation time series is a general name for the  
534 procedure of correcting and improving long-term modeled datasets by comparing  
535 them to short-term overlapping ground measurements. Different methodologies can  
536 be used for adapting a dataset of solar irradiance components to a specific site. Some  
537 solar data suppliers have even developed their own methods. Many methodologies are  
538 also inspired by bias removal techniques used in other fields of meteorology and  
539 climatology. Two main families of methodologies can be identified according to the  
540 purpose of the correction: regression-like methods and quantile mapping, from which  
541 emerges also the combination of both as a third family. The former method focuses on  
542 fitting by linear or multiple regressions the modeled data with ground data to an  
543 equation able to be applied to the whole dataset. The quantile mapping techniques  
544 work on the probability domain and correct the solar radiation data by fitting the  
545 distribution function of modeled data to the distribution function of observational  
546 data.

547

548 Under the framework of IEA-PVPS Task 16 a benchmarking exercise of site adaptation  
549 techniques has been conducted by several participants in a blind exercise. Ten sites  
550 and ten different measured and modeled pairs of datasets were prepared to test ten  
551 different methods for site adaptation. Satellite-derived and reanalysis-based solar  
552 irradiance data were included in the tested datasets to expand the variety of modeled  
553 data as much as possible.

554

555 The results of this assessment of techniques have shown that most techniques are able  
556 to produce improvement and some degree of correction of modeled data. There are,  
557 however, situations where the quality of modeled data is already very high, so that it is  
558 hard to get noticeable improvement in the site-adapted data. Nevertheless, quantile  
559 mapping techniques have shown the potential of removing the bias observed in  
560 modeled data. In addition, specific strategies that disaggregate the datasets according  
561 to the state of the sky (clear, non-clear, ranges of clear-sky index, etc.) may offer better  
562 performance. Likewise, the proper combination of techniques, such as sequential use  
563 of multiple regression and quantile mapping, also resulted in significant improvement  
564 in most situations.

565

566 In addition, a sensitivity analysis has been performed to study the proper training  
567 period of ground data and the impact of very high bias in atmospheric input (AOD is  
568 frequently overestimated or underestimated in some regions with a potential  
569 detrimental impact on modeled solar radiation). Thus, it can be observed that ground-  
570 based data time series covering periods of at least about one year seems to be  
571 appropriate for proper training of adaptation methodologies at most sites. Moreover,  
572 for the case of high bias in AOD-related quantities, quantile mapping based methods  
573 have shown very good performance regardless of the uncertainty in the atmospheric  
574 information used as input.

575

576 Finally, it is worth mentioning that it is difficult to establish a universal method or  
577 procedure that works with the same efficacy in all possible combinations of sites and  
578 modeled datasets. Good-quality ground data are always highly recommended for  
579 proper training. Statistical methodologies can be very efficient in adapting modeled  
580 data to a reference one, but in real conditions the better the quality of the reference  
581 (ground data) the higher the potential improvement. Moreover, bad-quality  
582 measurements could actually result in biased site adaptations, possibly more biased  
583 than the original modeled dataset. In addition, a preliminary analysis of the  
584 uncertainty at the site under scrutiny could be recommended before selecting one  
585 method or another and before designing the proper subsets of data onto which the  
586 site adaptation methodologies would be applied. It must be also remarked that even  
587 though in this work we have shown mostly a pure statistical procedure it is  
588 recommended to adapt only GHI and DNI and to compute DHI in a way that ensures  
589 the consistency among the three components and the closure relation. In fact, this was  
590 the procedure followed by Team 3 with two of the methods. Besides, it should be  
591 pointed out that not all the correction methods have been tested in this work and, in  
592 this sense, more methodologies, as model output statistics (MOS) and others, should  
593 be investigated in future studies. The number and climatic diversity of sites used for  
594 testing should also be increased to obtain results as universal as possible.

595

596 **Acknowledgements**

597 This work constitutes the main contribution of several experts to the activity 2.2 of the  
598 Task 16 IEA-PVPS and Task V IEA-SolarPACES. The authors wish to acknowledge also  
599 the collaborative work and efforts carrying out by all the experts and participants in  
600 the task, both in this activity as in many others, contributing to increase the knowledge  
601 and applications of solar resource characterization.

602

603 **References**

604

- 605 Amillo, A., Huld, T., Müller, R., 2014. A New Database of Global and Direct Solar Radiation  
606 Using the Eastern Meteosat Satellite, Models and Validation. *Remote Sensing* 6, 8165–  
607 8189. doi:10.3390/rs6098165
- 608 Armansperg, M. v., Oechslin, D., Schweneke, M., 2015. Financial Modelling of PV Risks.  
609 Financial Modelling of Technical Risks in PV Projects.
- 610 Bright, J.M., Sun, X., Gueymard, C.A., Acord, B., Wang, P., Engerer, N.A., 2020. Bright-Sun: A  
611 globally applicable 1-min irradiance clear-sky detection model. *Renewable and*  
612 *Sustainable Energy Reviews* 121, 109706. doi:10.1016/j.rser.2020.109706
- 613 Cannon, A.J., 2018. Multivariate quantile mapping bias correction: an N-dimensional  
614 probability density function transform for climate model simulations of multiple  
615 variables. *Climate Dynamics* 50, 31–49. doi:10.1007/s00382-017-3580-6
- 616 Cannon, A.J., Sobie, S.R., Murdock, T.Q., 2015. Bias Correction of GCM Precipitation by  
617 Quantile Mapping. *Journal of Climate* 28, 6938–6959.
- 618 Cano, D., Monget, J.M.M., Albuissou, M., Guillard, H., Regas, N., Wald, L., 1986. A method for  
619 the determination of the global solar radiation from meteorological satellite data. *Solar*  
620 *Energy* 37, 31–39. doi:10.1016/0038-092X(86)90104-0
- 621 Carta, J.A., Velázquez, S., Cabrera, P., 2013. A review of measure-correlate-predict (MCP)  
622 methods used to estimate long-term wind characteristics at a target site. *Renewable and*  
623 *Sustainable Energy Reviews*. doi:10.1016/j.rser.2013.07.004
- 624 Cros, S., Turpin, M., Aillaud, P., Lallemand, C., 2019. Real-time solar irradiance retrieval from  
625 satellite data: quality assessment of an operational tool using five satellites, in: 6th  
626 International Conference Energy & Meteorology. Copenhagen (Denmark).
- 627 Déqué, M., Rowell, D.P., Lüthi, D., Giorgi, F., Christensen, J.H., Rockel, B., Jacob, D., Kjellström,  
628 E., de Castro, M., van den Hurk, B., 2007. An intercomparison of regional climate  
629 simulations for Europe: assessing uncertainties in model projections. *Climatic Change* 81,  
630 53–70. doi:10.1007/s10584-006-9228-x
- 631 Feigenwinter, I., Kotlarski, S., Casanueva, A., Fischer, A.M., Schwierz, C., Liniger, M.A., 2018.  
632 Exploring quantile mapping as a tool to produce user-tailored climate scenarios for  
633 Switzerland. Technical Report MeteoSwiss, 270, 44 pp. 270.

- 634 Feng, F., Wang, K., 2019. Determining Factors of Monthly to Decadal Variability in Surface Solar  
635 Radiation in China: Evidences From Current Reanalyses. *Journal of Geophysical Research:*  
636 *Atmospheres* 124, 9161–9182. doi:10.1029/2018JD030214
- 637 Fernández-Peruchena, C.M., Vignola, F., Gastón, M., Lara-Fanego, V., Ramírez, L., Zarzalejo, L.,  
638 Silva, M., Pavón, M., Moreno, S., Bermejo, D., Pulgar, J., Macías, S., Valenzuela, R.X.,  
639 2018. Probabilistic assessment of concentrated solar power plants yield: The EVA  
640 methodology. *Renewable and Sustainable Energy Reviews* 91, 802–811.  
641 doi:10.1016/j.rser.2018.03.018
- 642 Fernández Peruchena, C.M., Ramírez, L., Silva-Pérez, M.A., Lara, V., Bermejo, D., Gastón, M.,  
643 Moreno-Tejera, S., Pulgar, J., Liria, J., Macías, S., Gonzalez, R., Bernardos, A., Castillo, N.,  
644 Bolinaga, B., Valenzuela, R.X., Zarzalejo, L.F., 2016. A statistical characterization of the  
645 long-term solar resource: Towards risk assessment for solar power projects. *Solar Energy*  
646 123, 29–39. doi:10.1016/j.solener.2015.10.051
- 647 Frank, C.W., Wahl, S., Keller, J.D., Pospichal, B., Hense, A., Crewell, S., 2018. Bias correction of a  
648 novel European reanalysis data set for solar energy applications. *Solar Energy* 164, 12–24.  
649 doi:10.1016/j.solener.2018.02.012
- 650 Guerreiro, L., Fernández-Peruchena, C.M., Cavaco, A., Gaston, M., Pereira, M.C., 2016.  
651 Experimental Validation of a Novel Methodology for Fast an Accurate Analysis of Solar  
652 Energy Yields Based on Cluster Analysis. *Proceedings of EuroSun2016* 1–8.  
653 doi:10.18086/eurosun.2016.09.03
- 654 Gueymard, C.A., 2011. Uncertainties in Modeled Direct Irradiance Around the Sahara as  
655 Affected by Aerosols: Are Current Datasets of Bankable Quality? *Journal of Solar Energy*  
656 *Engineering* 133, 031024, 1–13. doi:10.1115/1.4004386
- 657 Gueymard, C.A., 2012. Temporal variability in direct and global irradiance at various time  
658 scales as affected by aerosols. *Solar Energy* 86, 3544–3553.  
659 doi:10.1016/j.solener.2012.01.013
- 660 Gueymard, C.A., 2013. Aerosol turbidity derivation from broadband irradiance measurements:  
661 Methodological advances and uncertainty analysis. 42nd ASES National Solar Conference  
662 2013, SOLAR 2013, Including 42nd ASES Annual Conference and 38th National Passive  
663 Solar Conference 637–644.
- 664 Gueymard, C.A., 2014. A review of validation methodologies and statistical performance  
665 indicators for modeled solar radiation data: Towards a better bankability of solar  
666 projects. *Renewable and Sustainable Energy Reviews* 39, 1024–1034.  
667 doi:10.1016/j.rser.2014.07.117
- 668 Gueymard, C.A., Bright, J.M., Lingfors, D., Habte, A., Sengupta, M., 2019. A posteriori clear-sky  
669 identification methods in solar irradiance time series: Review and preliminary validation  
670 using sky imagers. *Renewable and Sustainable Energy Reviews* 109, 412–427.  
671 doi:10.1016/J.RSER.2019.04.027
- 672 Gueymard, C.A., Gustafson, W.T., Bender, G., Etringer, A., Storck, P., 2012. Evaluation of  
673 procedures to improve solar resource assessments: Optimum use of short-term data  
674 from a local weather station to correct bias in long-term satellite derived solar radiation  
675 time series. *World Renewable Energy Forum, WREF 2012, Including World Renewable*  
676 *Energy Congress XII and Colorado Renewable Energy Society (CRES) Annual Conferen* 3,  
677 2092–2099.

- 678 Hirsch, T., Dernasch, J., Fluri, T., García-Barberena, J., Giuliano, S., Hustig-Diethelm, F., Meyer,  
679 R., Schmidt, N., Seitz, M., Yildiz, E., 2017. SolarPACES Guideline for Bankable STE Yield  
680 Assessment. IEA Technology Collaboration Programme SolarPACES.
- 681 Huld, T., Paietta, E., Zangheri, P., Pinedo Pascua, I., 2018. Assembling Typical Meteorological  
682 Year Data Sets for Building Energy Performance Using Reanalysis and Satellite-Based  
683 Data. *Atmosphere* 9, 53. doi:10.3390/atmos9020053
- 684 Ines, A.V.M., Hansen, J.W., 2006. Bias correction of daily GCM rainfall for crop simulation  
685 studies. *Agricultural and Forest Meteorology* 138, 44–53.  
686 doi:10.1016/j.agrformet.2006.03.009
- 687 Izenman, A.J., 2016. *Modern Multivariate Statistical Techniques : regression, classification, and*  
688 *manifold learning*. Springer-Verlag New York.
- 689 Kothe, S., Hollmann, R., Pfeifroth, U., Träger-Chatterjee, C., Trentmann, J., Kothe, S., Hollmann,  
690 R., Pfeifroth, U., Träger-Chatterjee, C., Trentmann, J., 2019. The CM SAF R Toolbox—A  
691 Tool for the Easy Usage of Satellite-Based Climate Data in NetCDF Format. *ISPRS*  
692 *International Journal of Geo-Information* 8, 109. doi:10.3390/ijgi8030109
- 693 Lefèvre, M., Oumbe, A., Blanc, P., Espinar, B., Gschwind, B., Qu, Z., Wald, L., Schroedter-  
694 Homscheidt, M., Hoyer-Klick, C., Arola, A., Benedetti, A., Kaiser, J.W., Morcrette, J.-J.,  
695 2013. McClear: a new model estimating downwelling solar radiation at ground level in  
696 clear-sky conditions. *Atmos. Meas. Tech* 6, 2403–2418. doi:10.5194/amt-6-2403-2013
- 697 Long, C.N.N., Dutton, E.G.G., 2004. BSRN Global Network recommended QC tests, V2.0. BSRN  
698 Technical Report.
- 699 Mazorra Aguiar, L., Polo, J., Vindel, J.M.M., Oliver, A., 2019. Analysis of satellite derived solar  
700 irradiance in islands with site adaptation techniques for improving the uncertainty.  
701 *Renewable Energy* 135, 98–107. doi:10.1016/j.renene.2018.11.099
- 702 McGinnis, S., Nychka, D., Mearns, L.O., 2015. A New Distribution Mapping Technique for  
703 Climate Model Bias Correction, in: *Machine Learning and Data Mining Approaches to*  
704 *Climate Science*. Springer International Publishing, Cham, pp. 91–99. doi:10.1007/978-3-  
705 319-17220-0\_9
- 706 Merrouni, A.A., Ghennioui, A., Wolfertstetter, F., Mezrhab, A., 2017. The uncertainty of the  
707 HelioClim-3 DNI data under Moroccan climate. *AIP Conference Proceedings* 1850,  
708 140002–140011. doi:10.1063/1.4984519
- 709 Meyer, R., Schwandt, M., 2017. Documentation of Meteorological Data Sets delivered together  
710 with the SolarPACES Guideline for Bankable STE Yield Assessment, Version 2017.  
711 SolarPACES Report, [www.solarpaces.org/yield-analysis-guideline](http://www.solarpaces.org/yield-analysis-guideline).
- 712 Michelangeli, P.-A., Vrac, M., Loukos, H., 2009. Probabilistic downscaling approaches:  
713 Application to wind cumulative distribution functions. *Geophysical Research Letters* 36.  
714 doi:10.1029/2009GL038401
- 715 Molina, A., Falvey, M., Rondanelli, R., 2017. A solar radiation database for Chile. *Scientific*  
716 *Reports* 7, 14823. doi:10.1038/s41598-017-13761-x
- 717 Peng, X., She, J., Zhang, S., Tan, J., Li, Y., 2019. Evaluation of Multi-Reanalysis Solar Radiation  
718 Products Using Global Surface Observations. *Atmosphere* 10, 42.  
719 doi:10.3390/atmos10020042

- 720 Perdigão, J.C., Salgado, R., Costa, M.J., Dasari, H.P., Sanchez-Lorenzo, A., 2016. Variability and  
721 trends of downward surface global solar radiation over the Iberian Peninsula based on  
722 ERA-40 reanalysis. *International Journal of Climatology* 36, 3917–3933.  
723 doi:10.1002/joc.4603
- 724 Perez, R., Kivalov, S., Schlemmer, J., Hemker, K.J., Zelenka, A., 2010. Improving the  
725 performance of satellite-to-irradiance models using the satellite's infrared sensors. *Proc.*  
726 *of American Solar Energy Society Annual Conference*.
- 727 Perez, R., Schlemmer, J., Hemker, K., Kivalov, S., Kankiewicz, A., Gueymard, C., 2015. Satellite-  
728 to-Irradiance Modeling – A New Version of the SUNY Model, in: 42nd IEEE Photovoltaic  
729 Specialist Conference, At New Orleans, LA. doi:10.1109/PVSC.2015.7356212
- 730 Perez, R., Schlemmer, J., Kankiewicz, A., Dise, J., Tadese, A., Hoff, T., 2017. Detecting  
731 Calibration Drift at Reference Ground Truth Stations - A Demonstration of Satellite  
732 Irradiance Model's Accuracy, in: *IEEE PVSC-44*, Washington, DC.
- 733 Pfeifroth, U., Kothe, S., Müller, R., Trentmann, J., Hollmann, R., Fuchs, P., Werscheck, M., 2017.  
734 Surface Radiation Data Set - Heliosat (SARAH) - Edition 2.  
735 doi:10.5676/EUM\_SAF\_CM/SARAH/V002
- 736 Piani, C., Haerter, J.O., Coppola, E., 2010. Statistical bias correction for daily precipitation in  
737 regional climate models over Europe. *Theoretical and Applied Climatology* 99, 187–192.  
738 doi:10.1007/s00704-009-0134-9
- 739 Polo, J., Estalayo, G., 2015. Impact of atmospheric aerosol loads on Concentrating Solar Power  
740 production in arid-desert sites. *Solar Energy* 115, 621–631.  
741 doi:10.1016/j.solener.2015.03.031
- 742 Polo, J., Fernández-Peruchena, C., Gastón, M., 2017. Analysis on the long-term relationship  
743 between DNI and CSP yield production for different technologies. *Solar Energy* 115,  
744 1121–1129. doi:10.1016/j.solener.2017.07.059
- 745 Polo, J., Martín, L., Vindel, J.M., 2015. Correcting satellite derived DNI with systematic and  
746 seasonal deviations: Application to India. *Renewable Energy* 80, 238–243.  
747 doi:http://dx.doi.org/10.1016/j.renene.2015.02.031
- 748 Polo, J., Perez, R., 2019. Solar radiation modeling from satellite imagery, in: Polo, J.; Martín-  
749 Pomares, L., Sanfilippo, A. (Ed.), *Solar Resource Mapping - Fundamentals and*  
750 *Applications; Green Energy and Technology*. Springer, pp. 183–197. doi:10.1007/978-3-  
751 319-97484-2\_6
- 752 Polo, J., Téllez, F.M.M., Tapia, C., 2016a. Comparative analysis of long-term solar resource and  
753 CSP production for bankability. *Renewable Energy* 90, 38–45.  
754 doi:10.1016/j.renene.2015.12.057
- 755 Polo, J., Wilbert, S., Ruiz-Arias, J.A., Meyer, R., Gueymard, C., Sári, M., Martín, L., Mieslinger, T.,  
756 Blanc, P., Grant, I., Boland, J., Ineichen, P., Remund, J., Escobar, R., Troccoli, A., Sengupta,  
757 M., Nielsen, K.P., Renne, D., Geuder, N., Cebecauer, T., 2016b. Preliminary survey on site-  
758 adaptation techniques for satellite-derived and reanalysis solar radiation datasets. *Solar*  
759 *Energy* 132, 25–37. doi:10.1016/j.solener.2016.03.001
- 760 Polo, J., Zarzalejo, L.F., Ramirez, L., 2008. Solar radiation derived from satellite images, Chap.  
761 18. In: *Modeling Solar Radiation at the Earth Surface*, Chap. 18, in: *Modeling Solar*  
762 *Radiation at the Earth Surface*. Viorel Badescu. Springer-Verlag.



- 763 Porfirio, A.C.S., Ceballos, J.C., 2017. A method for estimating direct normal irradiation from  
764 GOES geostationary satellite imagery: Validation and application over Northeast Brazil.  
765 doi:10.1016/j.solener.2017.05.096
- 766 Posselt, R., Mueller, R.W., Stöckli, R., Trentmann, J., 2012. Remote sensing of solar surface  
767 radiation for climate monitoring - the CM-SAF retrieval in international comparison.  
768 Remote Sensing of Environment 118, 186–198. doi:10.1016/j.rse.2011.11.016
- 769 Qu, Z., Gschwind, B., Lefevre, M., Wald, L., Oumbe, A., Blanc, P., Espinar, B., Gesell, G.,  
770 Gschwind, B., Klüser, L., Lefèvre, M., Saboret, L., Schroedter-Homscheidt, M., Wald, L.,  
771 2017. Fast radiative transfer parameterisation for assessing the surface solar irradiance:  
772 The Heliosat-4 method. Meteorologische Zeitschrift 26, 33–57.  
773 doi:10.1127/metz/2016/0781
- 774 Ramirez Camargo, L., Dorner, W., 2016. Comparison of satellite imagery based data, reanalysis  
775 data and statistical methods for mapping global solar radiation in the Lerma Valley (Salta,  
776 Argentina). Renewable Energy 99, 57–68. doi:10.1016/j.renene.2016.06.042
- 777 Remund, J., Ramirez, L., Wilbert, S., Blanc, P., Lorenz, E., Köhler, C., Renné, D., 2017. Solar  
778 Resource for High Penetration and Large Scale Applications - A New Joint Task of IEA  
779 PVPS and IEA SolarPACES, in: Amsterdam, N. (Ed.), 33rd European Photovoltaic Solar  
780 Energy Conference and Exhibition PVSEC. pp. 14–15. doi:DOI:  
781 10.4229/EUPVSEC20172017-6BV.3.2
- 782 Richter, M., Kalisch, J., Schmidt, T., Lorenz, E., De Brabandere, K., 2015. Best Practice Guide On  
783 Uncertainty in PV Modelling.
- 784 Riihelä, A., 2018. Validation of the SARA-E Satellite-Based Surface Solar Radiation Estimates  
785 over India. Remote Sensing 10, 1–16. doi:10.3390/rs10030392
- 786 Salazar, G., Gueymard, C., Galdino, J.B., de Castro Vilela, O., Fraidenraich, N., 2020. Solar  
787 irradiance time series derived from high-quality measurements, satellite-based models,  
788 and reanalyses at a near-equatorial site in Brazil. Renewable and Sustainable Energy  
789 Reviews 117. doi:10.1016/j.rser.2019.109478
- 790 Sengupta, M., Habte, A., Gueymard, C., Wilbert, S., Renné, D., 2017. Best Practices Handbook  
791 for the Collection and Use of Solar Resource Data for Solar Energy Applications: Second  
792 Edition. doi:10.18777/ieashc-task46-2015-0001
- 793 Sengupta, M., Xie, Y., Lopez, A., Habte, A., Maclaurin, G., Shelby, J., 2018. The National Solar  
794 Radiation Data Base (NSRDB). Renewable and Sustainable Energy Reviews 89, 51–60.  
795 doi:10.1016/J.RSER.2018.03.003
- 796 Tahir, Z. ul R., Azhar, M., Blanc, P., Asim, M., Imran, S., Hayat, N., Shahid, H., Ali, H., 2020. The  
797 evaluation of reanalysis and analysis products of solar radiation for Sindh province,  
798 Pakistan. Renewable Energy 145, 347–362. doi:10.1016/j.renene.2019.04.107
- 799 Tang, W., Qin, J., Yang, K., Liu, S., Lu, N., Niu, X., 2016. Retrieving high-resolution surface solar  
800 radiation with cloud parameters derived by combining MODIS and MTSAT data.  
801 Atmospheric Chemistry and Physics 16, 2543–2557. doi:10.5194/acp-16-2543-2016
- 802 Themeßl, M.J., Gobiet, A., Heinrich, G., 2012. Empirical-statistical downscaling and error  
803 correction of regional climate models and its impact on the climate change signal.  
804 Climatic Change 112, 449–468. doi:10.1007/s10584-011-0224-4

805 Thomas, C., Saboret, L., Wey, E., Blanc, P., Wald, L., 2016. Validation of the new HelioClim-3  
806 version 4 real-time and short-term forecast service using 14 BSRN stations. *Advances in*  
807 *Science and Research* 13, 129–136. doi:10.5194/asr-13-129-2016

808 Trolliet, M., Walawender, J.P., Bourlès, B., Boilley, A., Trentmann, J., Blanc, P., Lefèvre, M.,  
809 Wald, L., 2018. Downwelling surface solar irradiance in the tropical Atlantic Ocean: a  
810 comparison of re-analyses and satellite-derived data sets to PIRATA measurements.  
811 *Ocean Science* 14, 1021–1056. doi:10.5194/os-14-1021-2018

812 Urraca, R., Gracia-Amillo, A.M., Huld, T., Martinez-De-Pison, F.J., Trentmann, J., Lindfors, A. V.,  
813 Riihelä, A., Sanz-Garcia, A., 2017. Quality control of global solar radiation data with  
814 satellite-based products. doi:10.1016/j.solener.2017.09.032

815 Urraca, R., Huld, T., Gracia-Amillo, A., Martinez-de-Pison, F.J., Kaspar, F., Sanz-Garcia, A., 2018.  
816 Evaluation of global horizontal irradiance estimates from ERA5 and COSMO-REA6  
817 reanalyses using ground and satellite-based data. *Solar Energy* 164, 339–354.  
818 doi:10.1016/J.SOLENER.2018.02.059

819 Wilcke, R.A.I., Mendlik, T., Gobiet, A., 2013. Multi-variable error correction of regional climate  
820 models. *Climatic Change* 120, 871–887. doi:10.1007/s10584-013-0845-x

821 Yang, D., 2018. A correct validation of the National Solar Radiation Data Base (NSRDB).  
822 *Renewable and Sustainable Energy Reviews* 97, 152–155.  
823 doi:10.1016/J.RSER.2018.08.023

824 Yang, D., 2019. Post-processing of NWP forecasts using ground or satellite-derived data  
825 through kernel conditional density estimation. *Journal of Renewable and Sustainable*  
826 *Energy* 11, 026101. doi:10.1063/1.5088721

827 Yang, D., Boland, J., 2019. Satellite-augmented diffuse solar radiation separation models.  
828 *Journal of Renewable and Sustainable Energy* 11, 023705. doi:10.1063/1.5087463

829 Yang, D., Perez, R., 2019. Can we gauge forecasts using satellite-derived solar irradiance?  
830 *Journal of Renewable and Sustainable Energy* 11, 023704. doi:10.1063/1.5087588

831 Zib, B.J., Dong, X., Xi, B., Kennedy, A., 2012. Evaluation and Intercomparison of Cloud Fraction  
832 and Radiative Fluxes in Recent Reanalyses over the Arctic Using BSRN Surface  
833 Observations. *Journal of Climate* 25, 2291–2305. doi:10.1175/JCLI-D-11-00147.1

834